Evidence for a break in the spectrum of astrophysical neutrinos

Luis A. Anchordoqui,[1,2,3,†] Martin M. Block,[4,*] Loyal Durand,[5,‡] Phuoc Ha,[6,§] Jorge F. Soriano,[1,2,‖] and Thomas J. Weiler[7,¶]

[1]*Department of Physics & Astronomy, Lehman College, City University of New York, New York 10468, USA*
[2]*Department of Physics, Graduate Center, City University of New York, New York 10016, USA*
[3]*Department of Astrophysics, American Museum of Natural History, New York 10024, USA*
[4]*Department of Physics & Astronomy, Northwestern University, Evanston, Illinois 60208, USA*
[5]*Department of Physics, University of Wisconsin, Madison, Wisconsin 53706, USA*[**]
[6]*Department of Physics, Astronomy, and Geosciences, Towson University, Towson, Maryland 21252, USA*
[7]*Department of Physics & Astronomy, Vanderbilt University, Nashville, Tennessee 37235, USA*

(Received 16 December 2016; published 21 April 2017)

The announcement by the IceCube Collaboration of the observation of 53 astrophysical neutrino candidates in the energy range $0.03 \lesssim E_\nu/\mathrm{PeV} \lesssim 2$ has been greeted with a great deal of justified excitement. Herein we provide fits of single and a broken power-law energy-spectra to these high-energy starting events (HESEs). By comparing our statistical results from fits to (background-free) shower HESE data with the spectral shape of muon neutrinos recently reported by the IceCube Collaboration, we show that there is (3σ) evidence for a break in the spectrum of astrophysical neutrinos. After that we use the fitted result to predict the rate of Glashow events (in the ≈6.3 PeV region) and *double-bang* tau neutrino events (in the PeV region) just at the threshold of IceCube detection.

DOI: 10.1103/PhysRevD.95.083009

I. INTRODUCTION

In 2012, the IceCube Collaboration reported the observation of two ∼1 PeV neutrinos, with a p-value 2.8σ beyond the hypothesis that these events were atmospherically generated [1]. The search technique was refined to extend the neutrino sensitivity to lower energies [2], resulting in the discovery of an additional 26 neutrino candidates with energies between 30 TeV and 2 PeV, constituting a 4.1σ excess for the combined 28 events compared to expectations from muon and neutrino atmospheric backgrounds produced by cosmic rays which strike the Earth's atmosphere [3]. With foresight (and luck) some of us used these early IceCube data to find the most probable neutrino spectral index, γ, assuming a single index describes the data, with the result $\gamma = 2.3$–2.4 [4]. Subsequent studies by the IceCube Collaboration with a larger data sample bolster our results [5].

At the time of writing, 54 "high-energy starting events" (HESE's), i.e. events initiated within the IceCube detector volume by entering neutrinos, have been reported in four years of IceCube data taking (1347 days between 2010–2014). With these events, a purely atmospheric explanation is rejected at more than 5.7σ [6]. The data are consistent with expectations for equal fluxes of all three neutrino flavors [7,8]. The analysis of all four years of data using an unbroken power law yields a best-fit spectral index of $\gamma = -2.58 \pm 0.25$, which is compatible with the 3-year result [6]. While the HESE flux above 200 TeV can be accommodated by a single power law with a spectral index $\gamma = 2.07 \pm 0.13$ [9], lowering the threshold revealed an excess of events in the 30–200 TeV energy range [5], raising the possibilities that the cosmic neutrino spectrum does not follow a single power law, and/or may be contaminated by an additional charmed particle background [10,11].

Indeed, quite recently the IceCube Collaboration reported a combined analysis based on six different searches for astrophysical neutrinos [12]. Assuming the neutrino flux to be isotropic and to consist of equal flavors at Earth, the all flavor spectrum with neutrino energies $25\ \mathrm{TeV} \leq E_\nu \leq 2.8\ \mathrm{PeV}$ is well described by an unbroken power law with best-fit spectral index -2.50 ± 0.09 and a flux at 100 TeV of $(6.7^{+1.1}_{-1.2}) \times 10^{-18}\ (\mathrm{GeV\,s\,sr\,cm^2})^{-1}$. Splitting the data into two sets, one from the northern sky and one from the southern sky, allows for a satisfactory power law fit with a different spectral index for each hemisphere. The best-fit spectral index in the northern sky was found to be $\gamma_N = 2.0^{+0.3}_{-0.4}$, whereas in the southern sky it was $\gamma_S = 2.56 \pm 0.12$. The discrepancy with respect to a single power law is found to be 1.1σ [12]. It is tempting to speculate that the different observed spectral indices (γ_N and γ_S) could be a harbinger of a real anisotropy between the two hemispheres. A lower energy contribution to the Southern hemisphere might be expected since much of the

*Deceased.
†luis.anchordoqui@gmail.com
‡ldurand@hep.wisc.edu
§pdha@towson.edu
‖jfdezsoriano@gmail.com
¶tom.weiler@vanderbilt.edu
**Present address: 415 Pearl Court, Aspen, CO 81611, USA.

Galactic plane (including its center [13]) lies in the Southern hemisphere [14]. An excess of lower energy events would push the spectral index of the single power-law Southern hemisphere to a larger $|\gamma_S|$ value. The hard spectral index γ_N is supported by a complimentary study using charged current muon neutrino events where the interaction vertex can be outside the detector volume [15]. This analysis, which includes IceCube data from 2009 through 2015 with the field of view restricted to the Northern hemisphere so that the Earth filters out atmospheric muons, suggests a neutrino spectrum $\propto E_\nu^{-(2.13\pm0.13)}$, for neutrino energies 191 TeV $\leq E_\nu \leq$ 8.3 PeV.

Independently of the presence or absence of the Galactic component of the astrophysical neutrino signal, a significant contribution to the flux could come from a population of extragalactic cosmic ray sources; for a review see e.g. [16].

To investigate possibilities, in this article we perform a study to constrain the spectral shape of the diffuse neutrino flux. Our intent is to establish whether or not a statistically significant break exists using data with reasonably well-known neutrino energies from 30 TeV to 10 PeV. This includes essentially the entire IceCube range, and as we know, the relative surplus of lower energy events and absence of events above 2.3 PeV give significant constraints on the spectrum. It is not our intent in this paper to provide an explanation for a break, if it exists. See [17–20] for some illustrative examples of two-component models.

The layout of the paper is as follows. In Sec. II we provide an overview of neutrino detection at IceCube, and describe the different event topologies resulting from the universal neutral current (NC) and individual charged current (CC) interactions of the three neutrino flavors. In Sec. III we describe the particulars of our likelihood approach and present spectral fits to the neutrino data. We display results from the analysis of HESE events initiated by electron and tau neutrinos, considering single and double exponential models. We also show a fit to the entire HESE data sample to ascertain whether the event topologies characteristics of muon showers are consistent with the fit including all particle species. As discussed below, knowledge of the incident muon neutrino energy E_ν does not predict the energy deposited in the IceCube detector by the muon track $E_\mu^{\rm dep}$, and vice versa; the statistical relation between the two is derived in Appendix A. Our analysis is similar in spirit and procedure to that in [21]. However, a key difference is that we consider only shower events, so that we have a sample of events free from atmospheric-background (even the ν_μ NC is not expected to give background events in our small sample). The trade off in lowered statistics is more than compensated by the purity of the sample events. Then, by comparing our shower-only analysis with the recent IceCube study on muon events, we are able to establish for the first time a break in the spectrum at the 3σ (99.7% CL) level. This evidence for the broken power law is our main result. The prospects for the not so distant future, including our predictions for the Glashow events [22] and *double-bang* tau neutrino events [23] from the Southern and Northern skies are presented in Sec. IV. The paper wraps up with some conclusions presented in Sec. V.

II. NEUTRINO INTERACTIONS AT ICECUBE

Neutrino (antineutrino) interactions in the Antarctic ice sheet can be reduced to three categories: (i) In CC interactions the neutrino becomes a charged lepton through the exchange of a $W^\pm$ with some nucleon N, $\nu_\ell(\bar\nu_\ell) + N \to \ell^\pm +$ anything, where lepton flavor is labeled as $\ell \in \{e, \mu, \tau\}$. (ii) In NC interactions the neutrino interacts via a Z transferring momentum to jets of hadrons, but producing a neutrino rather than a $\ell^\pm$ in the final state: $\nu_\ell(\bar\nu_\ell) + N \to \nu_\ell(\bar\nu_\ell) +$ anything. The scattered ν_ℓ exits the detector, carrying away energy, and so the observed energy presents a lower bound for the incident ν_ℓ energy. All three neutrino flavors exhibit a NC. These two possibilities are then projected onto two kinds of IceCube topologies to yield the three final possibilities: (i) "Shower" ($\mathcal{S}$) events result from all three flavors of NC events, and from the CC events of the electron and tau neutrinos below ~2 PeV. Shower events (also called "cascade" events) refer to the fact that energy is deposited no charged tracks (produced by muons or taus) are observed. (ii) Below a few PeV, "track" ($\mathcal{T}$) events are produced only by the muon neutrino CC. The ν_μ CC creates a muon and a hadronic shower within the IceCube detector, the muon track contributes to the deposited energy, but then the muon is seen to exit the detector as a single track of unknown energy. The deposited energy is only a lower bound to the incident muon neutrino energy.

At ν_τ energies above 3 PeV, ν_τ CC interactions begin to produce separable *double bang* events [23], with one smaller-energy shower produced by the initial ν_τ collision in the ice, and the second larger-energy shower resulting from the subsequent τ decay. At the lower energies of the data to which we fit, the showers tend to overlap one another and so are not discernible; at the energies of our fits, the ν_e's and ν_τ's are virtually indistinguishable (see, however, [24]). The correlations between the (NC, CC) $\otimes$ ($\mathcal{S}$, $\mathcal{T}$) are shown in Table I.

The classification of observed events in different topologies is not always straightforward. While almost all NC ν_μ events are generally correctly classified as showers, a non-negligible number of CC ν_μ events, of both atmospheric

TABLE I. Event topology for each neutrino flavor.

Interaction type	e	μ	τ
CC	$\mathcal{S}$	$\mathcal{T}$	$\mathcal{S}$
NC	$\mathcal{S}$	$\mathcal{S}$	$\mathcal{S}$

and astrophysical origin, could be misclassified as showers if the muon has too little energy or is produced near the edge of the detector, escaping in both cases without enough energy deposited to be detected [5,7]. The effects of these misclassifications have been studied in great detail in Refs. [8,21]. While accounting for misclassifications increases the fraction of μ-neutrinos and may have influence on the flavor ratios, with present statistics it does not influence the shape of the spectrum for a shower plus track analysis [8]. We expect only small differences in the cases where only showers are analyzed. In light of this, we assume here the event topologies at face value as given in [6].

It is appropriate to compare the NC shower rate to the CC shower rate. For the reference SM cross sections, we choose the results from perturbative QCD calculations constrained by HERAPDF1.5 shown in Fig. 1. These cross sections have been the benchmarks adopted by the IceCube Collaboration [3]. In the SM, over the energy range we explore here, the NC cross section is 29% of the total cross section, and the CC cross section makes up the remaining 71%. Moreover, for the NC, the deposited shower energy in the SM is 25% of the incident neutrino energy on average, whereas for the CC, the deposited shower energy is 100% of the incident neutrino energy [25]. For an energy falling as power law with index γ, the ratio of NC to CC showers at fixed $E^{\rm dep}$ is therefore $\mathrm{NC/CC} = (\frac{3}{2})(\frac{29}{71})(0.25)^{\gamma}$, where the $\frac{3}{2}$ is due to all three flavors contributing to the NC showers, but just two flavors contributing to the CC showers. This ratio is smaller than 4% for $\gamma \geq 2$. In what follows, we account for the NC contribution by weighting the IceCube target mass with the cross sections shown in Fig. 1, and accept the few percent under/over estimate of the flux normalization resulting from uncertainties in the weightings.

We have the three categories of events at this point, CC and NC showers and CC tracks. For the CC HESE shower events, no track leaves the detector and $E^{\rm dep}$ equals the incident neutrino energy, E_ν. For the CC HESE track events, some energy leaves the detector in the muon track, and a statistical equation relates observed $E^{\rm dep}$ to E_ν, as given in Appendix A. Moreover, the muon neutrino events are plagued by atmospheric backgrounds (mainly at the lower energies). It is estimated that in the four years of data collection, for $E_\nu \gtrsim 30$ TeV, 12.6 ± 5.1 events are atmospherically-produced down-coming (Southern) background muons, and another $9.0^{+8.0}_{-2.2}$ events are atmospherically-produced neutrino events [6]. The ratio of atmospherically-produced ν_μ's to ν_e's is order ten [27], and so the atmospheric contamination that plagues the nonatmospheric ν_μ CC is not present for our sample of ν_e or ν_τ CC, or for the NC interactions of all flavors. Accordingly, we choose to analyze just two of the three original categories of events, namely the NC and CC shower events, and avoid the track events completely. Later in this paper we will analyze how CC muon track events would impact the results of the present shower analysis.

At the energies of existing data, ν_e's and ν_τ's are indistinguishable in their interactions. The electromagnetic cascade triggered by the CC interactions of ν_e and ν_τ ranges out quickly. Such a cascade produces a nearly spherical light profile, and therefore exhibits a low angular resolution of about 15° to 20° [3]. However, a fully or mostly contained shower event provides a relatively precise measurement of the $\nu_{e/\tau}$ energy, with a resolution of $\Delta(\log_{10} E_\nu) \approx 0.26$ [28]. We note that the quality of the energy and angle inference is reversed for the CC interactions of ν_μ induced events. In this case, the secondary muon leaves behind a track of Cherenkov light of length a km or more. Muon tracks point nearly in the direction of the original ν_μ, allowing one to infer the arrival direction from the observed track with high angular resolution (say ~0.7°). On the other hand, the *electromagnetic equivalent energy deposited* $E_\mu^{\rm dep}$ represents only a lower bound on the genuine ν_μ energy. The authentic ν_μ energy may be up to a factor 5 larger than the deposited energy. NC interactions of all ν flavors also produce showers, but with a rate 60% (i.e. $\frac{3}{2} \times \frac{29}{71}$) that of CC

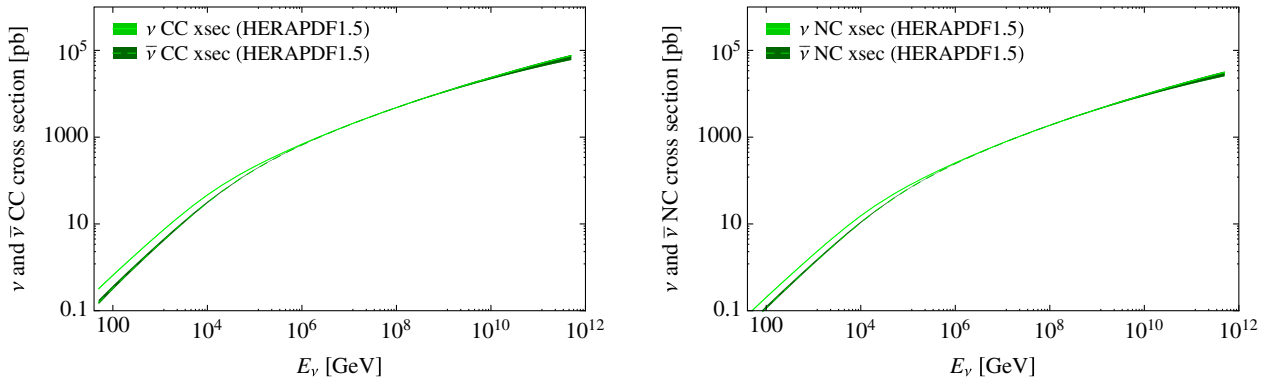

FIG. 1. Neutrino and antineutrino cross sections on isoscalar targets for CC and NC scattering according to HERAPDF1.5; $\sigma_{\rm CC}$ and $\sigma_{\rm NC}$, respectively. Taken from Ref. [26].

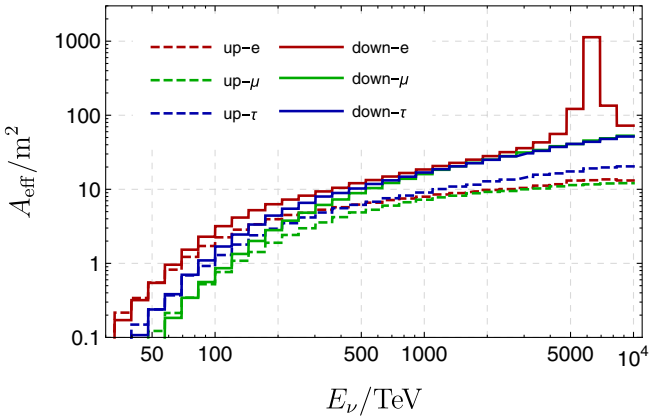

FIG. 2. IceCube effective areas for the different neutrino species.

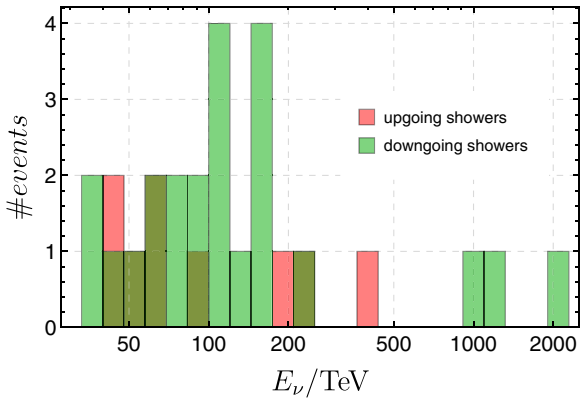

FIG. 3. Number distributions for up-and down-going HESE events. (Each dark "event" is an overlap of two events, one upgoing and the other down-going.)

interactions at the same incident neutrino energy, and with a much smaller shower energy [i.e. $(0.25)^\gamma$], as we have already noted.

Each of these mentioned effects, and the geometric particulars of the IceCube detector, are included in the effective areas for HESE events which have been published by the IceCube Collaboration [3] and are shown in Fig. 2. Conveniently, these $A_{\rm eff}(E_\nu)$'s are separated into those for the Northern hemisphere (up-going for IceCube at the South Pole) and those for the Southern hemisphere (down-going for IceCube). Included in this separation of effective areas is the absorption of up-going (Northern) neutrinos by the Earth matter. Thus, the systematics differ for the Northern and Southern neutrinos, but is encapsulated in the $A_{\rm eff}(E_\nu)$'s. (What is not included in the $A_{\rm eff}(E_\nu)$ of ν_μ is the relation between $E_\mu^{\rm dep}$ and E_{ν_μ}, which we provide in Appendix A).

In our analysis we use the full 1347-day HESE sample which contains 54 events. One of the events observed in the third year (event #32) was produced by a coincident pair of background muons from unrelated cosmic ray air showers and has now been excluded from the sample. The remaining events can be classified according to the arrival direction into North and South. Herein we use the best fit of the arrival direction to define the North and South subsamples. Out of the 53 events, 39 are showers. In our analysis we remove the low energy events by setting an energy threshold $E_\nu \geq 10^{1.52}$ TeV $\simeq 33.11$ TeV. Above this energy there are 32 showers and 14 tracks, the latter events including atmospheric background. The numbers for up- and down-going shower events are 9 and 23, respectively. The energy distribution of these numbers are shown in Fig. 3.

To summarize this section, for the energy range of present data, there are two different topologies for the events registered at IceCube, namely tracks and showers. The number of track events is expected to be smaller than the number of shower events by factor of ∼6, and the background for the track events at lower energies is formidable. The CC and NC origins of these topologies are summarized in Table I.

In the next section we present a full-likelihood approach to fit the CC and NC shower IceCube data sample, which allows us to constrain the shape of the energy spectrum of astrophysical neutrinos.

III. LIKELIHOOD ANALYSIS

Armed with IceCube observations we now perform the analysis to extract neutrino flux parameters using a maximum likelihood method. For completeness, we first write the most general form for the likelihood function and then we particularize the study to the different situations of interest.

Let $\boldsymbol{\theta}$ be the set of parameters involved in the data analysis, containing all the relevant guidelines to vary the incident flux. E.g. the $\boldsymbol{\theta}$ may be the normalization and spectral index of the power-law fit. Let $\bar{N}^{\mathcal{Z}}_{x,k}$ be the measured number of events with topology $\mathcal{Z} \in \{\mathcal{S}, \mathcal{T}\}$ and hemispherical direction $x \in \{u, d\}$ in the energy bin k. The probability that the bin k contains $\bar{N}^{\mathcal{Z}}_{x,k}$ events of type $(x, \mathcal{Z})$ while expecting $N^{\mathcal{Z}}_{x,k}(\boldsymbol{\theta})$ is given by a Poisson distribution

$$\mathcal{P}[\bar{N}^{\mathcal{Z}}_{x,k}|N^{\mathcal{Z}}_{x,k}(\boldsymbol{\theta})] = \frac{e^{-N^{\mathcal{Z}}_{x,k}}(N^{\mathcal{Z}}_{x,k})^{\bar{N}^{\mathcal{Z}}_{x,k}}}{\bar{N}^{\mathcal{Z}}_{x,k}!}, \tag{1}$$

while the probability that the bin k contains $\bar{N}^{\mathcal{Z}}_{x,k}$ events of type $(x, \mathcal{Z})$ for all the types is

$$\mathcal{P}_k(\boldsymbol{\theta}) \equiv \prod_{x,\mathcal{Z}} \mathcal{P}[\bar{N}^{\mathcal{Z}}_{x,k}|N^{\mathcal{Z}}_{x,k}(\boldsymbol{\theta})]. \tag{2}$$

The likelihood of having a given a set of parameters $\boldsymbol{\theta}$ observing the actual event distribution is

$$\mathcal{L}(\boldsymbol{\theta}) = \prod_k \mathcal{P}_k(\boldsymbol{\theta}). \quad (3)$$

By the maximization of $\mathcal{L}$ in terms of the parameters $\boldsymbol{\theta}$ we will estimate the most likely values for those parameters. The logarithm of the likelihood is often taken to ensure that we work with sums instead of with products. Thus, as an alternative formulation, maximization of $\mathcal{L}$ becomes minimization of $-\ln\mathcal{L}(\boldsymbol{\theta})$. We have $-\ln\mathcal{P}_k = \sum_{x,\mathcal{Z}}[N^{\mathcal{Z}}_{x,k} + \bar{N}^{\mathcal{Z}}_{x,k}\ln(N^{\mathcal{Z}}_{x,k}) - \ln(\bar{N}^{\mathcal{Z}}_{x,k}!)]$. The latter term, $-\ln(\bar{N}^{\mathcal{Z}}_{x,k}!)$, may be continued as a Gamma function: $-\ln\Gamma(\bar{N}^{\mathcal{Z}}_{x,k}+1)$. Notice that in bins where there are zero events, the log-likelihood still receives a nonzero contribution $\sum_{x,\mathcal{Z}} N^{\mathcal{Z}}_{x,k}$ (The Poisson likelihood for an empty bin is $e^{-\sum_{x,\mathcal{Z}} N^{\mathcal{Z}}_{x,k}}$).

The expected number of events per bin is given by

$$N^{\mathcal{Z}}_{x,k}(\theta) = 2\pi T \int_k \Phi_j(E_\nu,\theta) A^{\mathcal{Z}}_x(E_\nu,\theta) dE_\nu, \quad (4)$$

where, Φ_j is the diffuse neutrino flux per flavor and per particle/antiparticle, with j taking values in $\{\nu_e,\bar{\nu}_e,\nu_\mu,\bar{\nu}_\mu,\nu_\tau,\bar{\nu}_\tau\}$, and $A^{\mathcal{Z}}_x$ is the effective area in the kth energy bin, and where $\int_k$ represents the integration along that bin. For sufficiently narrow bins in $\ln E_\nu$, it can easily be shown that the integral is well approximated by

$$N^{\mathcal{Z}}_{x,k}(\boldsymbol{\theta}) = 2\pi T \langle A^{\mathcal{Z}}_x\rangle_k \int_k \Phi_j(E_\nu,\boldsymbol{\theta}) dE_\nu \quad (5)$$

where $\langle A^{\mathcal{Z}}_x\rangle_k$ is the averaged effective area for $(x,\mathcal{Z})$. For local power-law descriptions of the effective area and the flux, the corrections are of order Δ_k^2, where Δ_k is the width of bin k. These corrections are negligible for the IceCube bins. The nonaveraged effective areas for $(x,\mathcal{Z})$ events are obtained as

$$A^{\mathcal{Z}}_x = \sum_{(i,\ell)\in\mathcal{Z}} A^{i,\ell}_x. \quad (6)$$

Here i labels the interaction type (charged or neutral current) and ℓ labels the neutrino flavor, and sums are extended to the values allowed by Table I for each topology. Finally, $A^{i,\ell}_x = \omega^{i,\ell} A^\ell_x$, being A^ℓ_x the effective areas accompanying [3]. The weights $\omega^{i,\ell}$ can be calculated from the target-mass data (also in [3]) as

$$\omega^{i,\ell} = \frac{\eta_i M^\ell_i}{\sum_k \eta_k M^\ell_k}, \quad (7)$$

with $\eta_i \equiv \sigma_i/\sigma_{TOT}$ as given in Fig. 1.

First we perform an approach which finesses the inevitable statistical uncertainty in $E^{\rm dep}_\mu/E_{\nu_\mu}$, by simply omitting the track events from the data sample. Assuming equal representations of the three neutrino flavors in the incident neutrino flux, Monte Carlo simulations reveal the ratio of (up-going) track events at fixed $E^{\rm dep}_\mu$ to be of order 1/6 in IceCube [29].[1] Thus, the loss of event statistics due to omission of track events is small, of order 17%.

A. Unbroken power law

We first hypothesize that the cosmic neutrino flux per flavor and per particle/antiparticle, averaged over all three flavors, follows an unbroken power law of the form

$$\Phi_j(E_\nu) \equiv \frac{dF_j}{dE_\nu dA d\Omega dt} = \Phi_0 (E_\nu/E_0)^{-\gamma} = \Phi_0 \exp[-\gamma \ln(E_\nu/E_0)], \quad (8)$$

where the normalization energy scale, $E_0 \simeq 33.11$ TeV, is fixed by the low energy bound of the first used energy bin above 30 TeV.

The single power flux (8) can be integrated to obtain

$$\int_k \Phi_i(E_\nu,\boldsymbol{\theta}) dE_\nu = \frac{2\Phi_0 E_0}{\gamma-1}\left(\frac{\langle E\rangle_k}{E_0}\right)^{1-\gamma} \sinh\frac{(\gamma-1)\Delta}{2}, \quad (9)$$

where

$$\Delta \equiv \ln\left(\frac{E^k_{\rm max}}{E^k_{\rm min}}\right) \quad \text{and} \quad \langle E\rangle_k \equiv \sqrt{E^k_{\rm min} E^k_{\rm max}}. \quad (10)$$

Note that for the logarithmically spaced bins, Δ is a constant. For our bin choice, $\Delta = 0.08\ln(10) \approx 0.18$.

At this stage it is worthwhile to point out that for energies above about 2 PeV the spectral index γ must be steeper than 2.4 for 1σ consistency with the nonobservation of Glashow $\bar{\nu}_e + e^- \to W^-$ events at 6.3 PeV [30].

For an unbroken power law, the parameters are $\boldsymbol{\theta} = \{\Phi_0,\gamma\}$, for a given reference energy E_0. $\mathcal{L}(\Phi_0,\gamma)$ can be maximized, using north and south hemisphere shower data. The 1, 3, and 5σ confidence contours are displayed in Fig. 4. After marginalizing the relevant parameters our results can be summarized as follows:

$$\Phi_0 = (0.91^{+0.33}_{-0.25}) \times 10^{-9}\ \text{TeV}^{-1}\,\text{m}^{-2}\,\text{sr}^{-1}\,\text{s}^{-1} \quad (11)$$

and

$$\gamma = 3.10^{+0.22}_{-0.20}. \quad (12)$$

In Figs. 5 and 6 we show the local and cumulative number distributions compared to the data. We note that displaying the fit results in this form have some advantages over the

[1] *A priori* one would expect the rate to reflect the equal flavor ratios, ~1/3, but systematic differences in $E^{\rm dep}_\mu$ from track and shower produce another suppression factor of ~1/2.

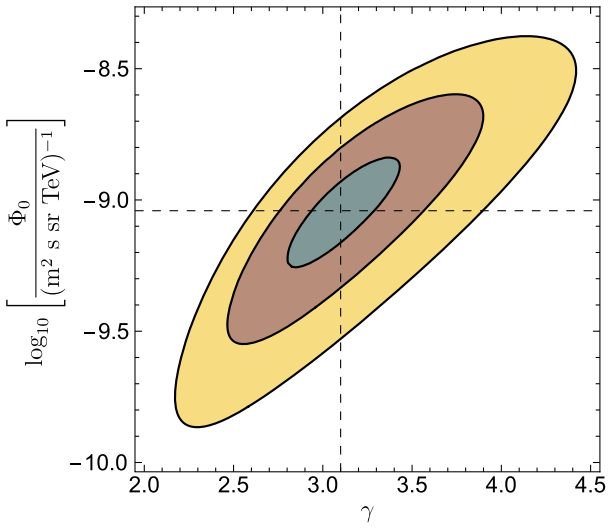

FIG. 4. 1, 3, and 5σ confidence contours for (Φ_0, γ).

usual log plots of $E_\nu^2\Phi_j(E_\nu)$ with points and error bars. This is because the number distribution is what is actually measured, and the bins with zero numbers cannot be displayed. It is difficult to judge the significance of the results when one's eyes just follow the flux curve and the nonzero data points.

On the other hand, we note that plotting of $E_\nu^2\Phi_j(E_\nu)$ versus log E_ν conserves the area under a spectrum even after processing the electromagnetic cascade of accompanying γ rays. Thus, for optically thin Waxman-Bahcall (WB) sources [31], where we expect roughly equal fluxes of photons and neutrinos, the area of the π^0 contribution to the isotropic diffuse γ-ray spectrum provides an upper bound to the $\pi^\pm$ origin of the neutrinos.

As shown in Fig. 7 there is tension between the preferred soft spectral index (12) and the harder spectrum of the isotropic γ ray emission measured by Fermi-LAT [32]. (The tension explicitly visible in Fig. 7 has also been predicted using numerical simulations [33].) As of today, this

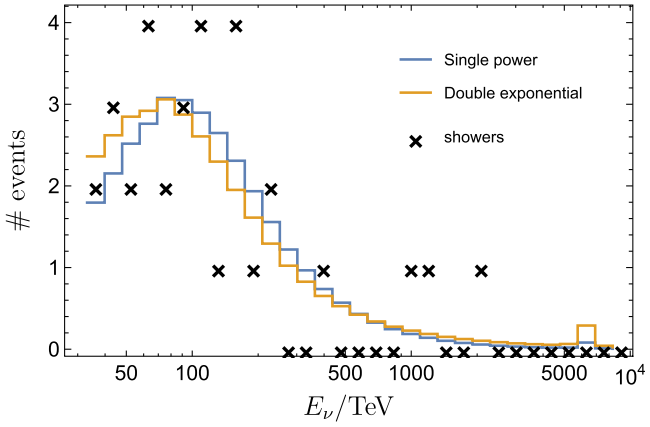

FIG. 5. Histogram of showers, predicted and measured.

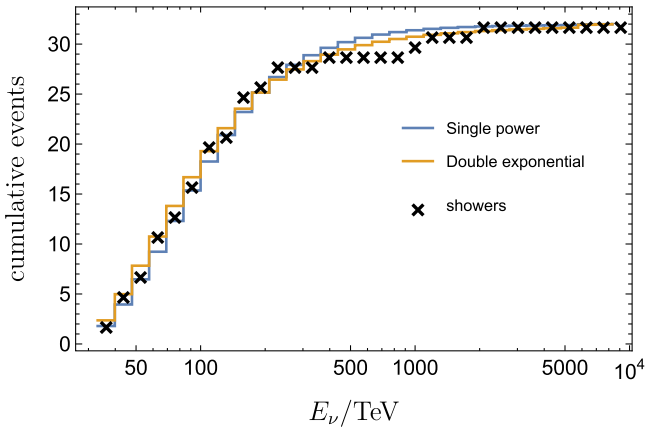

FIG. 6. Cumulative histogram of showers, predicted and measured.

represents the strongest constraint. It actually rules out the unbroken power law hypothesis on the assumption that IceCube's neutrinos are produced via pion decay in optically thin sources. The tension between (12) and Fermi-LAT data can be relaxed if, for example, a significant component of the IceCube flux originates in neutron β-decay [34]. However, such a possibility is presently strongly disfavored by the observed neutrino flavor ratios [7]. Alternatively, one can argue that the extragalactic neutrino sources are hidden, that is, they are opaque to the emission of γ rays and/or cosmic rays producing the neutrino flux [35]. Therefore, it is interesting to ascertain whether the HESE data by itself imply a break in the spectrum of astrophysical neutrinos.

B. Fitting the single power law with showers and tracks

To ascertain the impact of ν_μ CC interactions in our analysis, we redo the single power law analysis including the track events (without subtracting background from tracks). As already noted, the deposited energy is not the same as the energy of the parent neutrino. One approximation is to assign an energy for the parent neutrino of each track event, as explained in the Appendix A. Otherwise, we proceed exactly as before. For the single power law model we obtain for the shower plus track events

$$\Phi_0 = (1.1 \pm 0.3) \times 10^{-9}\ \mathrm{TeV}^{-1}\,\mathrm{m}^{-2}\,\mathrm{sr}^{-1}\,\mathrm{s}^{-1} \quad (13)$$

and

$$\gamma = 3.08^{+0.17}_{-0.16}. \quad (14)$$

Looking at (12) and (14), we see that our assumption that misclassification of CC ν_μ introduces a negligible effect is justified when considering only shower events. This concludes the analysis justifying our assumption that misclassification of events does not induce significant changes in the spectral shape.

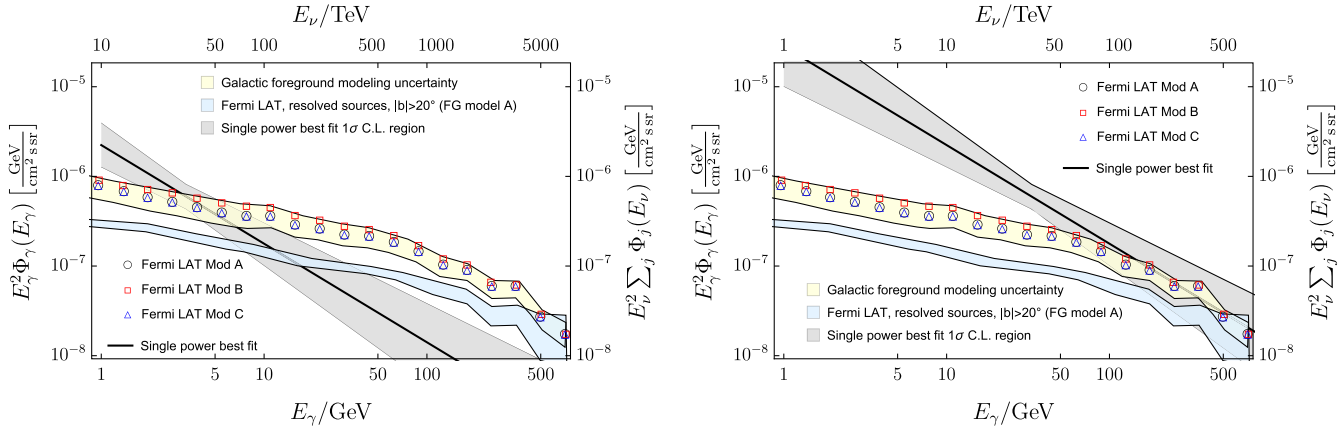

FIG. 7. The open symbols represent the total extragalactic γ-ray background for different foreground (FG) models as reported by the Fermi Collaboration [32]. For details on the modeling of the diffuse Galactic foreground emission in the benchmark FG models A, B and C, see [32]. The cumulative intensity from resolved Fermi LAT sources at latitudes $|b| > 20°$ is indicated by a (grey) band. The best fit to IceCube's shower data (left) and its extrapolation down into the TeV-energy range (right) assuming an unbroken power law, is also shown for comparison.

It is important to stress that for an unbroken power law, spectral indices $\lesssim$2.5 are excluded at 99.7% CL (from both the shower and the shower + track analyses). Note, however, that the IceCube analysis of the muon neutrino spectrum favors an index somewhat harder: $\gamma = 2.13 \pm 0.13$ [15]. This index is 3σ-incompatible ($2.13 + 3\times 0.13 = 2.52$) with our single power law shower and shower + track analyses, thereby providing 3σ evidence for a break in the spectrum of astrophysical neutrinos.[2]

C. Two-exponential model

In this section we describe the broken power law of incident neutrino flux by the sum of two exponentials in $\log E_\nu$, or equivalently by two powers of E_ν,

$$\Phi_j(E_\nu) \equiv \Phi_0\left[\left(\frac{E_\nu}{E_0}\right)^{-\gamma_1} + \sigma\left(\frac{E_\nu}{E_0}\right)^{-\gamma_2}\right], \qquad (15)$$

with $0 < \sigma < 1$.

We duplicate our analysis using the maximum likelihood method to extract the values of the parameters that maximize the probability that the observed number distributions are described by the assumed flux, for up- and down-going shower events. The best values of the flux parameters are found to be

$$\Phi_0 = (1.1^{+0.6}_{-0.7}) \times 10^{-9}\ \mathrm{TeV^{-1}\,m^{-2}\,sr^{-1}\,s^{-1}}, \qquad (16)$$

and

$$\gamma_1 = 3.63^{+4.96}_{-0.85}, \qquad \gamma_2 = 2.43^{+6.83}_{-0.92}, \qquad \sigma = 0.0827^{+7}_{-0.0821}. \qquad (17)$$

The high upper uncertainties observed in the parameters are due to the flatness of the likelihood function, which comes from the fact that an increase in one of the parameters can be compensated by decrease in some of the others to produce an equally likely fit. For example, a large value of Φ_0 can be compensated by a value of σ low enough to keep the adequate normalization of the γ_2 term, and with a very large γ_1, which will make the first term in (15) falls rapidly with increasing energy and not contribute at all to the events over 33 TeV. This basically reduces the fit to a single power-law with exponent γ_2 and normalization $\sigma\Phi_0$. Note that the upper uncertainty of the σ parameter goes into the unphysical region, $\sigma > 1$. In Figs. 5 and 6 we show the local and cumulative number distributions for the double exponential model compared to the data.

The significance ($\sim 1.1\sigma$) for the existence of a spectral break in HESE data is thus comparable to the one obtained by the IceCube Collaboration splitting a larger data set into northern and southern subsamples [12]. It is interesting to note that the expected number of events above 912 TeV for the double exponential model is 1.84, while 3 are observed. The Poisson probability for this to happen is 0.165. On the other hand, for a single power law form, the fit predicts that above the same energy 1.013 events are expected, with an associated Poisson probability of 0.063. All in all, for the most likely parameter values, the double exponential is roughly more probable by a factor of $0.165/0.063 \approx 2.6$ than the unbroken power-law.

The break energy is obtained when both flux components are equal. This condition reads

$$E_{\mathrm{break}} = E_0\sigma^{(\gamma_2-\gamma_1)^{-1}}. \qquad (18)$$

As a practical matter, given the current limited statistics, we determine the break energy using the most probable

[2]Actually, the statistical significance resulting from (12) is $2.93\sigma \simeq 3\sigma$.

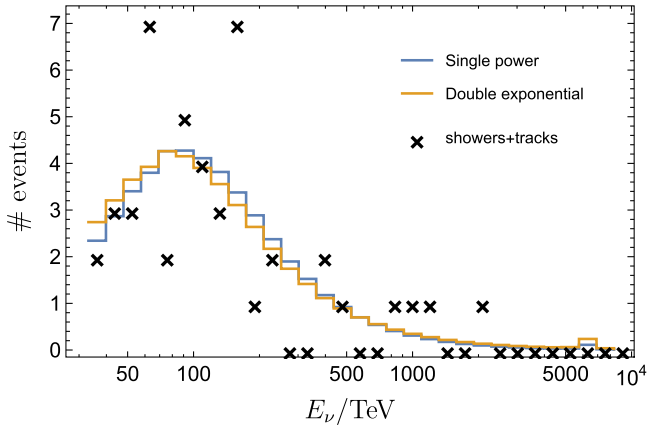

FIG. 8. Histogram of events, predicted and measured.

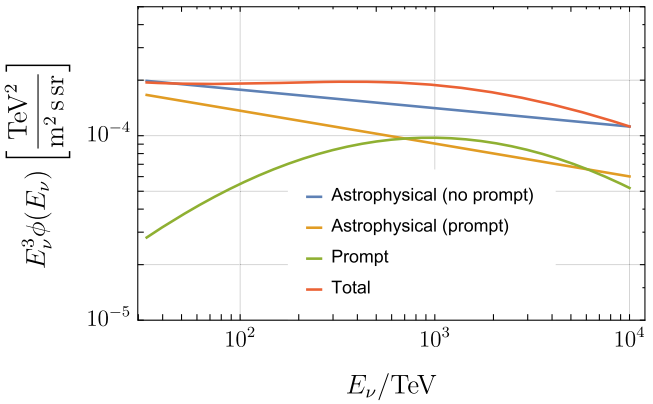

FIG. 10. Prompt, astrophysical and prompt + astrophysical total fluxes for the single-exponential (showers only).

parameter values, yielding $E_{\text{break}} \approx 263$ TeV. This break energy is consistent with the results of [21].

The double exponential model favors the following parameter values

$$\Phi_0 = (1.1^{+0.6}_{-0.7}) \times 10^{-9}\ \text{TeV}^{-1}\,\text{m}^{-2}\,\text{sr}^{-1}\,\text{s}^{-1} \qquad (19)$$

and

$$\gamma_1 = 3.47^{+2.97}_{-0.70}, \qquad \gamma_2 = 2.62, \qquad \sigma = 0.17. \qquad (20)$$

The results of the likelihood fits can be observed in the histograms and cumulative histograms shown in Figs. 8 and 9. The break energy is $E_{\text{break}} \approx 266$ TeV. It is noteworthy that the confidence intervals of γ_2 and σ do not close at 68% C.L. and therefore the result is consistent with an unbroken power law at the 1σ level.

D. Impact of the prompt neutrino flux

A source of events that could bias our analysis is the neutrino flux originated by the prompt decay of charmed particles in the atmosphere. At present, there is a large systematic uncertainty in the determination of the prompt neutrino flux. For the lower limit of the allowed prompt neutrino intensity, one would expect no modification to our previous study. In order to analyze how a large flux of prompt neutrino might alter our results, we repeat the analysis of previous sections assuming the other extreme, i.e. throughout this section we adopt a prompt flux that saturates the upper limit for forward charm production [10,11].

The fits are done following the same procedure but with slight modifications in (5): (i) now, the total flux is the sum of an astrophysical flux component and a parameter-independent prompt flux (i.e. it contains no dependence on the fit parameters), and (ii) the flux produced by the charmed particles is flavor dependent [10,11]. The prompt component has to be corrected to account for the IceCube self-veto applied to the effective areas as defined in (6); this point is further detailed in Appendix B. After taking care of these details, we obtain the results for the fluxes shown in Figs. 10–13. A comparison with the results from previous sections (blue lines) is also shown in these figures.

The presence of the prompt component clearly decreases the total amount of events due to the astrophysical flux, as

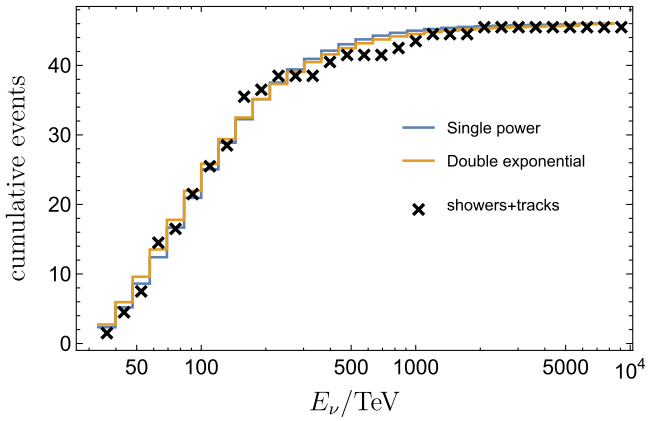

FIG. 9. Cumulative histogram of events, predicted and measured.

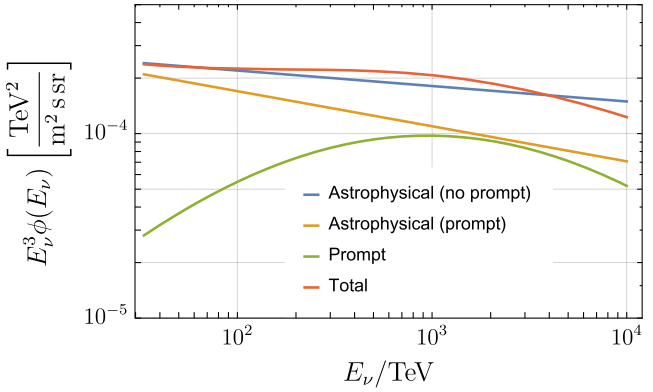

FIG. 11. Prompt, astrophysical and prompt + astrophysical total fluxes for the single-exponential (showers and tracks).

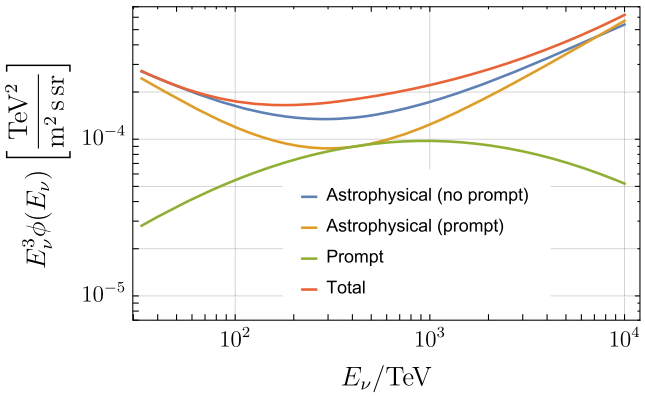

FIG. 12. Prompt, astrophysical and prompt + astrophysical total fluxes for the double-exponential (showers only).

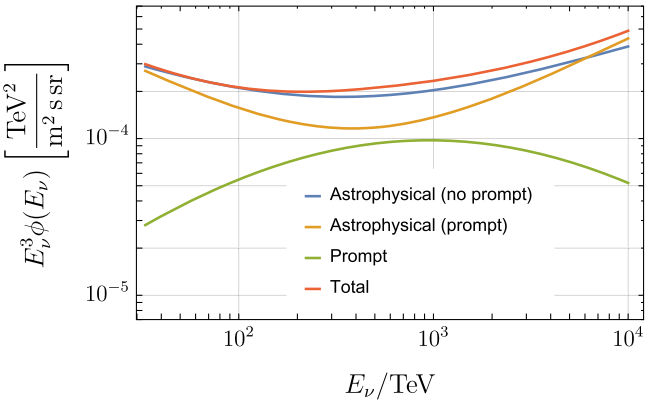

FIG. 13. Prompt, astrophysical and prompt + astrophysical total fluxes for the double-exponential (showers and tracks).

can be seen both in the single and double exponential cases. Nevertheless, its energy dependence favors the power law break in double exponential models, as can be appreciated in Figs. 12 and 13. The changes on the exponents in both models are show in Table II. The energy break is displaced up to 290 TeV for showers and 390 TeV for showers and tracks, approximately.

It is important to emphasize the agreement of our results with those obtained in [10,11] in the fact that the prompt flux cannot explain the observed event distribution. In all the cases the astrophysical flux tends to dominate the spectrum at the highest energies, and only in the case of single exponential without tracks the prompt flux dominates the spectrum along some energy range.

TABLE II. Impact of the prompt flux on power laws.

Fit model	Without prompt	With prompt
Single, $\mathcal{S}$	3.10	3.18
Single, $\mathcal{S}+\mathcal{T}$	3.08	3.19
Double, $\mathcal{S}$	(3.63, 2.42)	(3.78, 2.28)
Double, $\mathcal{S}+\mathcal{T}$	(3.47, 2.62)	(3.60, 2.38)

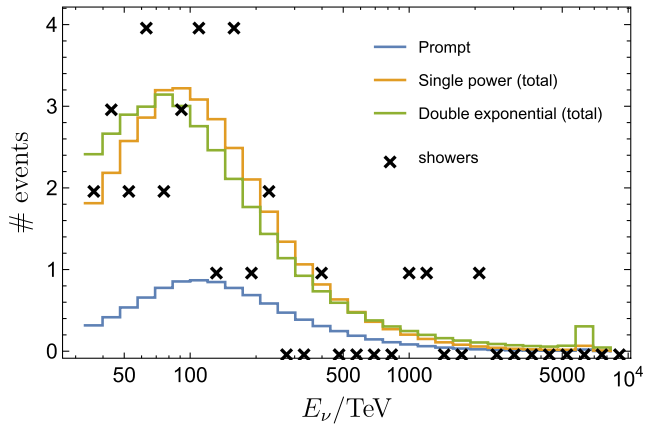

FIG. 14. Histogram of events, predicted and measured, including prompt events (showers).

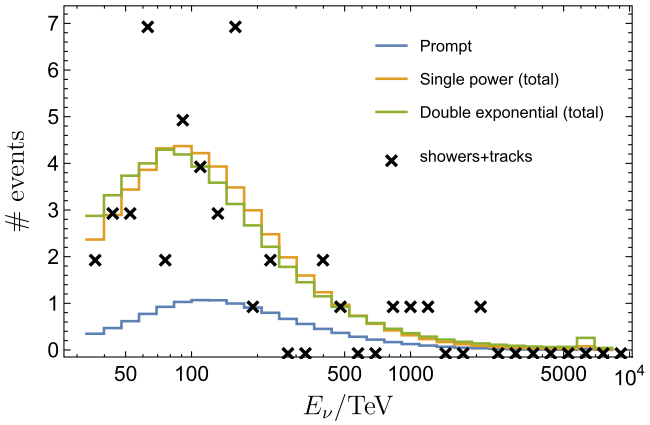

FIG. 15. Histogram of events, predicted and measured, including prompt events (showers and tracks).

Finally, in Figs. 14 and 15 we show the final distribution of events. As one can see in Table II, for a single exponential, the effect of the prompt neutrino flux is to make the astrophysical neutrino spectrum steeper, and therefore our main conclusion from Sec. III B (there is a 3σ evidence for a break in the spectrum) remains unaltered.

E. Glashow resonometer

The rate of interaction of ν_e, ν_μ, ν_τ, $\bar{\nu}_\mu$, $\bar{\nu}_\tau$ with electrons is mostly negligible compared to interactions with nucleons. However, the case of $\bar{\nu}_e$ is unique because of resonant scattering, $\bar{\nu}_e + e^+ \to W^- \to$ anything, at $E_\nu \simeq 6.3$ PeV [22]. As noted elsewhere [36], the signal for $\bar{\nu}_e$ at the Glashow resonance, when normalized to the total $\nu + \bar{\nu}$ flux, can be used to possibly differentiate between the two primary candidates ($p\gamma$ and pp collisions) for neutrino-producing interactions in optically thin sources of cosmic rays. In pp collisions, the nearly isotopically neutral mix of pions will create on decay a neutrino population with the ratio $N_{\nu_\mu} = N_{\bar{\nu}_\mu} = 2N_{\nu_e} = 2N_{\bar{\nu}_e}$. On the other hand, in

photopion interactions the isotopically asymmetric process $p\gamma \to \Delta^+ \to \pi^+ n$, $\pi^+ \to \mu^+ \nu_\mu \to e^+ \nu_e \bar{\nu}_\mu \nu_\mu$ is the dominant source of neutrinos so that at production, $N_{\nu_\mu} = N_{\bar{\nu}_\mu} = N_{\nu_e} \gg N_{\bar{\nu}_e}$ (assuming little π^- "contamination"). It is therefore of interest to consider situations in which the flux of neutrinos is equally divided among the three flavors, but with a negligible component of $\bar{\nu}_e$. To account for this possibility we consider an effective area which does not contain effects from the Glashow resonance. This will allow harder exponents in the high energy component.

The results of the likelihood fit assuming a single exponential model are

$$\Phi_0 = (1.2^{+0.4}_{-0.3}) \times 10^{-9}\ \mathrm{TeV}^{-1}\,\mathrm{m}^{-2}\,\mathrm{sr}^{-1}\,\mathrm{s}^{-1} \quad (21)$$

and

$$\gamma = 3.17^{+0.22}_{-0.21} \quad (22)$$

for shower events, and

$$\Phi_0 = (1.4^{+0.4}_{-0.3}) \times 10^{-9}\ \mathrm{TeV}^{-1}\,\mathrm{m}^{-2}\,\mathrm{sr}^{-1}\,\mathrm{s}^{-1}, \quad (23)$$

with

$$\gamma = 3.14^{+0.18}_{-0.17}, \quad (24)$$

for showers and tracks together.

For the double exponential model, we obtain

$$\Phi_0 = (1.6^{+0.7}_{-0.7}) \times 10^{-9}\ \mathrm{TeV}^{-1}\,\mathrm{m}^{-2}\,\mathrm{sr}^{-1}\,\mathrm{s}^{-1}, \quad (25)$$

and

$$\gamma_1 = 3.63^{+0.90}_{-0.40}, \qquad \gamma_2 = 2.03^{+0.86}_{-0.84}, \qquad \sigma = 0.0159^{+2}_{-0.0155}, \quad (26)$$

for showers, and

$$\Phi_0 = (1.7^{+0.7}_{-1.0}) \times 10^{-9}\ \mathrm{TeV}^{-1}\,\mathrm{m}^{-2}\,\mathrm{sr}^{-1}\,\mathrm{s}^{-1}, \quad (27)$$

and

$$\gamma_1 = 3.5, \qquad \gamma_2 = 2.3, \qquad \sigma = 0.04, \quad (28)$$

for showers and tracks. Note that for showers, the upper uncertainty of the σ parameter again goes into the unphysical ($\sigma > 1$) region. Moreover, once more when showers and tracks are considered in the fit, the confidence intervals of γ_1, γ_2, and σ do not close at 68% C.L. and therefore the result is consistent with a single, unbroken power law at the 1σ level. The energy break is $E_{\mathrm{break}} \approx 440$ TeV in the fit to shower data and $E_{\mathrm{break}} \approx 490$ TeV for showers and tracks. The results form the likelihood fits can be observed in Figs. 16, 17, 18 and 19.

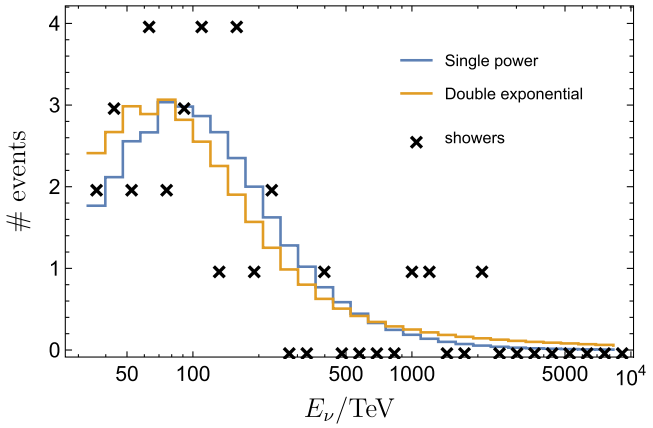

FIG. 16. Histogram of showers, predicted and measured, without Glashow resonance.

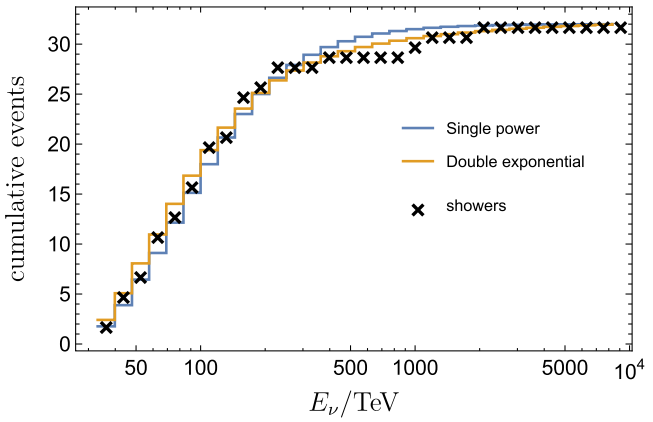

FIG. 17. Cumulative histogram of showers, predicted and measured, without Glashow resonance.

It is important to stress that the expected number of events above 912 TeV for the double exponential model is 2.167, with a Poisson probability of 0.194. For the unbroken power law assumption, the fit predicts that above

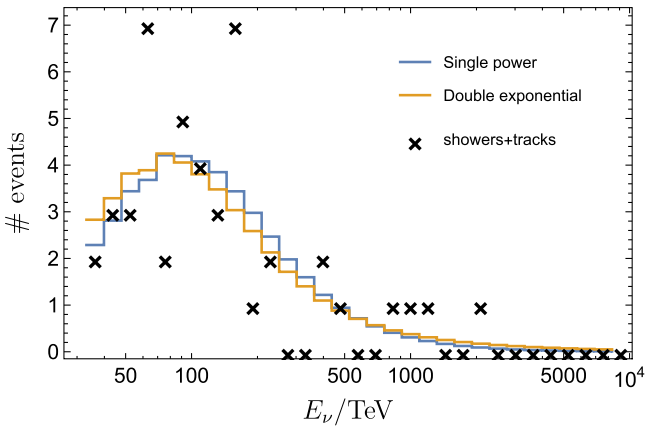

FIG. 18. Histogram of showers and tracks, predicted and measured, without Glashow resonance.

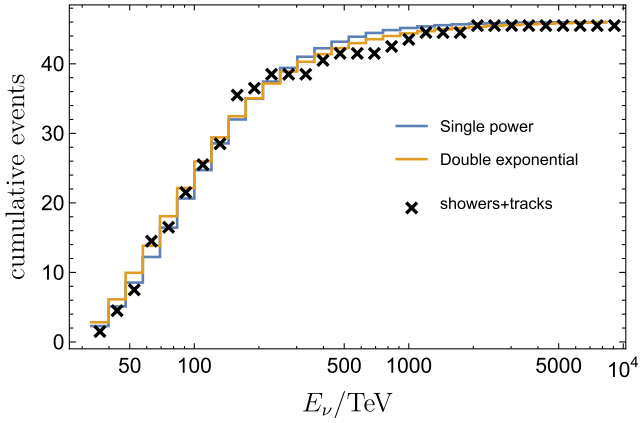

FIG. 19. Cumulative histogram of showers and tracks, predicted and measured, without Glashow resonance.

the same energy 0.899 events are expected, with an associated Poisson probability of 0.049. Altogether, the double exponential is about $0.194/0.049 \sim 4$ times more probable than the unbroken power law.

IV. LOOKING AHEAD WITH ICECUBE-GEN2

In the very near future, two more years of IceCube data, 2014–2016, are expected to be unblinded. Looking farther into the future, design studies for the IceCube-Gen2 high-energy array are well underway [37]. They will result in an instrumented volume approaching 10 km^3 and will lead to significantly larger neutrino detection rates, across all neutrino flavor and detection channels.[3] A rough estimate indicates about an order of magnitude increase in exposure per year. The bigger instrumented volume will facilitate the calorimetric detection of muon tracks, reducing significantly the systematic uncertainty. The extension will reuse the very reliable design of IceCube's digital optical modules and therefore it will surely perform technologically at least at the level of IceCube. A conservative estimate of the sample size is then attainable by simply scaling the instrumented volume.

In 4 years of observation, IceCube has detected 54 events with incident neutrino energy above above 25 TeV. Of these, about 20 events have energies in the range 100 TeV $< E_\nu <$ 2 PeV. This detection rate implies that in 10 years of data taken by the IceCube facility will collect on the order of 50 neutrino events within this (roughly) decade of energy. The next generation of neutrino telescope in the South pole, IceCube-Gen2, will increase the per year exposure by about an order of magnitude, and therefore in 10 year's of observation will collect roughly 500 neutrinos with 100 TeV $< E_\nu <$ 2 PeV.

We have noted that *double bang* and Glashow events could play a key role in constraining processes of neutrino production. It seems then reasonable to extrapolate the fluxes derived in the previous section to estimate the event rate at IceCube-Gen2. The search for *double bang* events is possible above 3 PeV. Therefore, we fix the search bins by $2.8 < E_\nu/\text{PeV} < 10$ and determine the yearly event rate assuming the favored parameters for the double exponential model. If the neutrino flux is democratically distributed among flavors and particle-antiparticle, we expect 0.3 *double bang* events per year at IceCube-Gen2, whereas if the $\bar{\nu}_e$ component is suppressed, we expect 0.7 *double bang* events per year. On the other hand, for Glashow events, we search in the resonance bins $4 < E_\nu/\text{PeV} < 10$ shown in Fig. 2. As we can see, the numbers of ν_τ, $\bar{\nu}_\tau$, and $\bar{\nu}_e$ events are correlated. Therefore, by comparing the rates of Glashow events and *double bang* events, one will be able to study flavor as well as particle-antiparticle ratios.

V. CONCLUSIONS

The most pressing consequence of IceCube's discovery of astrophysical neutrinos is that the flux level observed is exceptionally high by astronomical standards. The magnitude of the observed flux is at a level of the WB bound [31] which applies to neutrino production in optically thin sources that are responsible for emission of ultrahigh energy cosmic rays. In this paper we have performed a study to constrain the spectral shape of the diffuse neutrino flux and obtain information on possible source environments. Our results are encapsulated in Figs. 4 to 19, and are summarized in these concluding remarks:

(i) We have conducted our study using data from events produced by CC interactions of tau and electron neutrino flavors as well as NC interactions of all neutrino flavors, but avoiding the background-laden ν_μ CC track events. The "shower" data have essentially no atmospheric background, and at the same time allows a precise determination of the relation between the energy deposited in the detector and the original neutrino energy. The total atmospheric muon background in four years of data is found to be 12.6 ± 5.1 [6], while the background from atmospheric neutrinos reported by the IceCube Collaboration, presumed to be overwhelmingly ν_μ's, which through their CC produce track topologies [27], is $9.0^{+8.0}_{-2.2}$ [6].

(ii) If astrophysical neutrinos originate in WB sources, the tension between IceCube and Femi-LAT data stands as a strong constraint for the hypothesis of an unbroken power law describing the spectrum in the energy range 10 TeV $\lesssim E_\nu \lesssim$ 10 PeV. By analyzing IceCube's HESE data sample we have found clues for a break in the spectrum at $200 \lesssim E_{\text{break}}/\text{TeV} \lesssim 500$, independently of the neutrino origin(s). Using Poisson statistics we have shown that if the flux of neutrinos at Earth is democratically

[3]This may be complemented by atmospheric neutrino telescopes [38].

distributed among both flavors and particle-antiparticle, then the description of the spectrum with an apparent break is roughly 2.6 times more probable than the unbroken power law. We have also shown that if the flux of $\bar{\nu}_e$ is significantly suppressed with respect to other neutrino species, so as to suppress resonant production of Glashow events 6.3 PeV, then the description of the spectrum with the apparent break is about 4 times more probable than the unbroken power law.

(iii) The IceCube Collaboration has recently released a study using CC muon neutrino events, with interaction vertex outside the detector volume [15]. Because of the large muon range the effective area for track topologies is significantly larger than in the HESE sample. The price paid is that $E^{\rm dep}$ is only statistically related to a range of incident neutrino energies. The data collected from 2009 through 2015 is well described by a Monte-Carlo generated isotropic, unbroken power law flux with a normalization at 100 TeV neutrino energy of $(0.90^{+0.30}_{-0.27} \times 10^{-18}\ \mathrm{GeV\,cm^2\,s\,sr})^{-1}$ and a spectral index of $\gamma = 2.13 \pm 0.13$. This hard spectrum is consistent with that expected in Fermi engines [39]. Our likelihood fit for a neutrino flux democratically distributed among flavors and particle-antiparticle, yields $\gamma_2 \approx 2.43$; the result of the IceCube Collaboration is not inconsistent with our findings. This is because the likelihood function for γ_2 is rather flat due to limited statistics; for all the cases analyzed in this paper, the fitted γ_2 is consistent with a Fermi engine at the 68% CL. On the other hand, we have shown that for an unbroken power law, spectral indices $\lesssim$2.5 are excluded at 99.7% CL. Requiring the IceCube analysis of the ν_μ spectral index to be compatible with the shower analysis presented here provides additional evidence (3σ effect) for a break in the spectrum of astrophysical neutrinos.

(iv) A similar study to determine the spectral shape has been presented in [21]. However, unlike the study of [21], our statistical analysis becomes background free by using only shower events. In such a background free analysis, the slope of the spectrum for the unbroken power-law hypothesis, $\gamma = 3.10^{+0.22}_{-0.20}$, is somewhat steeper than the result obtained in [21], which is $\gamma = 2.84^{+0.25}_{-0.27}$. Our analysis differs from [21] in that we obtain smaller errors on the neutrino spectral index by sacrificing some data in favor of background-free HESE data. Though the results are compatible at the 1σ level, by direct comparison with the ν_μ IceCube spectrum ($\gamma = 2.13 \pm 0.13$), we see that only the resulting softer shower spectrum and smaller errors resulting from our analysis allows us to extract (3σ) evidence for a break in the cosmic neutrino spectrum. For the two-exponential model, the results of the two studies are also compatible within errors.

(v) IceCube has proposed a larger next-generation detector [37]. IceCube-Gen2 will surely have a technology at least as sophisticated as the first generation IceCube, so a conservative estimate of the future sample size is attainable by simply scaling apertures. IceCube-Gen2 will have an order of magnitude larger aperture than IceCube, so one can expect the clarity that comes with at least an order of magnitude more astrophysical neutrino data. By extrapolating the flux for a double exponential model we have shown that if the neutrino flux is democratically distributed among flavors and particle-antiparticle, then the new South pole facility will observe about 1 Glashow event per year and about 0.1 *double bangs* per year. If on the other hand the flux of $\bar{\nu}_e$ is significantly suppressed with respect to the other neutrino species, then the rate of *double bangs* becomes about 0.7 events per year. Thus by comparing the rates of Glashow and *double bang* events one can study not only flavor ratios, but also particle-antiparticle ratios. Such analyses are key to understanding source properties.

In summary, by confronting the favored parameters of our likelihood fit to shower events assuming an unbroken power law with the hard ν_μ spectrum recently announced by the IceCube Collaboration, we have shown that there is evidence for a break in the spectrum of astrophysical neutrinos, sustained by a 3σ discrepancy among the predicted spectral indices by these two analyses. This is our main conclusion. The localization of the break-energy is at present hampered by the limited available statistics. However, we have shown that the favored parameters of our likelihood fit assuming a double exponential model provide a favored break in the $200 \lesssim E_{\rm break}/\mathrm{TeV} \lesssim 500$ range.

ACKNOWLEDGMENTS

We thank Francis Halzen for guidance throughout much of this work, and Subir Sarkar for permission to reproduce Fig. 1. M. M. B., L. D., and T. J. W. would like to thank the Aspen Center for Physics for its hospitality and for its partial support of this work under NSF Grant No. 1066293. L. A. A. is supported by NSF Grant No. PHY-1620661 and by NASA Grant No. NNX13AH52. G. P. H. would like to thank the Towson University Fisher College of Science and Mathematics for support. The research of T. J. W. was supported in part by DoE Grant No. DE-SC0011981. J. F. S. was partially supported by the grant Ayudas de movilidad del personal docente e investigador 2015, from Universidad de Alcalá; he thanks María D. Rodríguez Frías and Luis del Peral for their support needed to start this work.

APPENDIX A: ENERGY-DEPENDENT MUON ABSORPTION

As explained in Sec. II, at the energies of present IceCube HESE data, NC and CC interactions of the neutrinos deposit all their energy into shower energies, except for the CC interaction of the muon neutrino. For HESE ν_μ events, a track begins in the IceCube detector, but usually continues beyond the detector's border. We wish to know the relation between the incident neutrino energy E_ν and the energy deposited $E_\mu^{\rm dep}$ in the IceCube detector. To this end, we begin with the differential equation for the muon energy loss in a medium.

$$\frac{dE_\mu}{d\ell} = -(a + bE_\mu), \tag{A1}$$

where a and b are slowly varying functions of muon energy E_μ that also depend on the medium in which the muon propagates. The coefficient a characterizes the ionization losses of the muon, and b characterizes the other losses due to brehmsstrahlung, e^+e^- pair production, nuclear interactions. For muon transit through ice at energies in the 30 TeV to 2 PeV range, we follow [40] and take $a = 0.28$ TeV/km and $b = 0.28$/km (and so $a/b = 1$ TeV). Although the true energy losses are known to be stochastic rather than continuous, the average values characterized by a and b parameters which we use in the continuous loss formula above are quite accurate [41]. The solution to Eq. (A1) is

$$E_\mu(\ell) + \frac{a}{b} = \left[E_\mu(0) + \frac{a}{b}\right] e^{-b\ell}. \tag{A2}$$

The deposited energy from muon losses over the detector distance ℓ is then

$$E_\mu^{\rm dep} = E_\mu(0) - E_\mu(\ell) = \left[E_\mu(0) + \frac{a}{b}\right](1 - e^{-b\ell}). \tag{A3}$$

The number of events due to an incident muon-neutrino of energy E_ν, with deposited energy $E_\mu^{\rm dep}$, is

$$\frac{d^2N}{dE_\mu^{\rm dep} dE_{\nu_\mu}} = (\Delta\Omega T)(A_{\rm eff}^{\nu_\mu}(E_\nu)\Phi_{\nu_\mu}(E_\nu)) \int_{E_\mu^{\rm dep}}^{E_\nu} dE_\mu(0) \left[\frac{1}{\sigma_{\rm CC}} \frac{d\sigma_{\rm CC}}{dE_\mu(0)}(E_\mu(0), E_\nu)\right] \times \int_{\ell_{\rm min}}^{\ell_{\rm max}} \frac{d\ell}{L} \delta\left\{E_\mu^{\rm dep} - \left[\left(E_\mu(0) + \frac{a}{b}\right)(1 - e^{-b\ell})\right]\right\}. \tag{A4}$$

The length integral here averages the distance traveled by the muon in the detector, and so $L = \ell_{\rm max} - \ell_{\rm min}$. We take $\ell_{\rm min} = 300$ m so that an identifiable track is produced [42] and take $\ell_{\rm max}$ equal to the IceCube detector size of 1 km. (For future use, we note that these choices imply the values $(1 - e^{-b\ell_{\rm max}}) = 0.244$, and $(1 - e^{-b\ell_{\rm min}}) = 0.081$.)

In fact the deposited energy includes a hadronic contribution. We define $E^{\rm dep} = E_\mu^{\rm dep} + E_{\rm had}$, and turn to the commonly used y-distribution notation for simplicity. One defines $y \equiv E_{\rm had}/E_\nu$. Then it follows that $E_\mu(0) = (1 - y)E_\nu$, and one has $E_{\rm had} = yE_\nu$, and

$$E^{\rm dep} = \left[(1 - y)E_\nu + \frac{a}{b}\right](1 - e^{-b\ell}) + yE_\nu. \tag{A5}$$

We arrive at

$$\frac{d^2N}{dE^{\rm dep} dE_{\nu_\mu}} = (\Delta\Omega T)(A_{\rm eff}^{\nu_\mu}(E_\nu)\Phi_{\nu_\mu}(E_\nu)) \int_0^1 dy \left[\frac{1}{\sigma_{\rm CC}} \frac{d\sigma_{\rm CC}}{dy}(y, E_\nu)\right] \times \int_{\ell_{\rm min}}^{\ell_{\rm max}} \frac{d\ell}{L} \delta\left\{E^{\rm dep} - \left[\left((1 - y)E_\nu + \frac{a}{b}\right)(1 - e^{-b\ell}) + yE_\nu\right]\right\}. \tag{A6}$$

The integration limits on y follow from $E^{\rm dep} = E_\mu^{\rm dep} + E_{\rm had}$, where $y = 1$ corresponds to pure $E^{\rm dep} = E_{\rm had}$, and $y = 0$ corresponds to pure $E^{\rm dep} = E_\mu^{\rm dep}$.

Note that the δ-function may be written

$$\frac{\delta\{\ell - \ell_0\}}{b(E_\nu + a/b - E^{\rm dep})}, \tag{A7}$$

where the root $\ell_0(E_\nu, y, E^{\rm dep})$ is the effective range for the muon

$$\ell_0 = \frac{1}{b}\ln\left(\frac{E_\nu + a/b - yE_\nu}{E_\nu + a/b - E^{\rm dep}}\right) \approx \frac{1}{b}\ln\left(\frac{(1-y)}{1 - E^{\rm dep}/E_\nu}\right). \tag{A8}$$

The second rendition ignores the small term $a/b \sim$ TeV. We remark that as a check, the argument of the

logarithm is always greater than one, so the log is always positive.

The $d\ell/L$ integral over the δ-function is easily done analytically to yield $[(Lb)(E_\nu + a/b - E^{\rm dep})]^{-1}$, while from $\ell_{\rm min} \le \ell_0 \le \ell_{\rm max}$ come the additional integration limits

$$y_{\rm min} \le y \le y_{\rm max} \tag{A9}$$

with

$$y_{\rm min} \equiv \left(\frac{(E_\nu + a/b)(1 - e^{+b\ell_{\rm max}}) + E^{\rm dep} e^{+b\ell_{\rm max}}}{E_\nu}\right) \quad \text{and}$$
$$y_{\rm max} \equiv \left(\frac{(E_\nu + a/b)(1 - e^{+b\ell_{\rm min}}) + E^{\rm dep} e^{+b\ell_{\rm min}}}{E_\nu}\right). \tag{A10}$$

The new extent of the y-range is $\Delta y \equiv (y_{\rm max} - y_{\rm min}) = (e^{+b\ell_{\rm max}} - e^{+b\ell_{\rm min}})(E_\nu + a/b - E^{\rm dep})/E_\nu$. We have

$$\frac{d^2N}{dE^{\rm dep} dE_{\nu_\mu}} = \frac{(\Delta\Omega T)}{(Lb)(E_\nu + \frac{a}{b} - E^{\rm dep})} (A_{\rm eff}^{\nu_\mu}(E_\nu)\Phi_{\nu_\mu}(E_\nu)) \times \int_{(0,y_{\rm min})}^{(1,y_{\rm max})} dy \left[\frac{1}{\sigma_{\rm CC}} \frac{d\sigma_{\rm CC}}{dy}(y, E_\nu)\right]. \tag{A11}$$

Equation (A11) gives the allowed incident neutrino energies E_ν that can lead to the observed deposited energy $E^{\rm dep}$, and conversely, gives the deposited energy values $E^{\rm dep}$ that can result from an incident neutrino energy E_ν. The average neutrino energy giving rise to $E^{\rm dep}$ is readily obtained by integrating Eq. (A11) over E_ν and dividing by an appropriate ΔE_ν. Here's a parameter count: (i) The integration on y, or equivalently, choosing $\langle y\rangle$, eliminates y; we are left with independent $(E^{\rm dep}, E_\nu, \ell)$. (ii) Then integrating ℓ subject to the δ-function eliminates on more variable, so we are left with two independent variables. (iii) The condition for the peak of E_ν versus $E^{\rm dep}$ leaves just one independent variable, which we can take to be E_ν. Thus we have $E^{\rm dep}(E_\nu)$, or $\ell(E_\nu)$. An approximate form of Eq. (A11) is obtained by setting y equal to its average value of $\langle y\rangle$, or equivalently, setting $d\sigma/dy = \sigma_0 \delta(y - \langle y\rangle)$. Then the final integral in Eq. (A11) equates to unity. The trivial result is

$$\frac{d^2N}{dE^{\rm dep} dE_{\nu_\mu}} = \frac{(\Delta\Omega T)(A_{\rm eff}^{\nu_\mu}(E_\nu)\Phi_{\nu_\mu}(E_\nu))}{(Lb)(E_\nu + a/b - E^{\rm dep})}. \tag{A12}$$

Since $A_{\rm eff}^{\nu_\mu}$ is rising with E_ν only logarithmically (see Fig. 2), and Φ_{ν_μ} is falling with E_ν like a power law, and the denominator is linearly rising with E_ν, we see that the allowed E_ν is not symmetric in its allowed region, but rather peaks at or near the lower limit.

Peak values of the exact Eq. (A11) or the approximate Eq. (A12) are given by equating the differentials $d(\ln \text{numerator})$ and $d(\ln \text{denominator})$; so we have

$$\frac{d\ln(A_{\rm eff}^{\nu_\mu}\Phi_{\nu_\mu}(E_\nu))}{dE_\nu} = \left(E_\nu + \frac{a}{b} - E^{\rm dep}\right)^{-1} \tag{A13}$$

as the equation which implicitly determines the peak value of E_ν. But $A_{\rm eff}^{\nu_\mu}(E_\nu)\Phi_{\nu_\mu}(E_\nu)$ is a decreasing function of E_ν, and hence its derivative with respect to neutrino energy is negative, but equated with $(E_\nu + a/b - E^{\rm dep})^{-1}$ which is positive. Thus the peak in the binning is backed up to the boundary value $(E_\nu)^{\rm bin\ min}$, which implies, $\ell = \ell_{\rm max}$. We get simply

$$(E^{\rm dep})_{\rm peak} = \langle y\rangle E_\nu + \left[(1 - \langle y\rangle)E_\nu + \frac{a}{b}\right](1 - e^{-b\ell_{\rm max}}), \tag{A14}$$

with $E_\nu = (E_\nu)^{\rm bin\ min}$. Typically, $b\ell_{\rm max}$ is $\mathcal{O}(0.3)$ and a/b is an ignorable $\mathcal{O}$(TeV), so accepting a 15% error in the (bracketed) second term on the right-hand side, we get finally

$$(E^{\rm dep})_{\rm peak} = [\langle y\rangle + (1 - \langle y\rangle)b\ell_{\rm max}](E_\nu)^{\rm bin\ min}. \tag{A15}$$

With $\langle y\rangle \sim 0.20$–$0.40$, one gets $(E^{\rm dep})_{\rm peak} \sim E_\nu/2$, with roughly half of the deposited energy arising from the hadronic deposition [the first term in Eq. (A15)], and half arising from the muonic deposition [the second term in Eq. (A15)]. The two terms on the right-hand side contribute equally at $\langle y\rangle = b\ell_{\rm max}/(1 + b\ell_{\rm max}) \sim 0.22$. Inverting Eq. (A15) is trivial; we have

$$\left(\frac{E_\nu}{E^{\rm dep}}\right)_{\rm peak} = \left(\frac{(E_\nu)^{\rm bin\ min}}{E^{\rm dep}}\right) = [\langle y\rangle + (1 - \langle y\rangle)b\ell_{\rm max}]^{-1}. \tag{A16}$$

The width at half-maximum is given by substituting the value of $E^{\rm dep}$ given in Eq. (A15) into Eq. (A12), setting E_ν in Eq. (A12) equal to $E_\nu + \Gamma$, and setting the entire value equal to $\frac{1}{2}$ of the peak value, i.e.

$$\frac{E_\nu + \Gamma}{E_\nu} = 2\frac{A_{\rm eff}\Phi_{\nu_\mu}(E_\nu + \Gamma)}{A_{\rm eff}\Phi_{\nu_\mu}(E_\nu)}. \tag{A17}$$

For example, if $A_{\rm eff}\Phi_{\nu_\mu}(E_\nu)$ behaves as a power law with index $E_\nu^{-\beta}$, then $\Gamma = (2^{1/(1+\beta)} - 1)E_\nu$; for $\beta = 3.5$, we get $\Gamma = 0.165E_\nu$, and for $\beta = 2.0$, we get $\Gamma = 0.260E_\nu$.

For ν scattering off of a valence quark (antiquark), helicity considerations give $\langle y\rangle = 1/2$ $(1/4)$, while for $\bar\nu$ scattering, $\langle y\rangle$ has the opposite values, $1/4$ $(1/2)$. Since the target is a combination of quarks and antiquarks, one might expect $\langle y\rangle$ to be bounded by $0.5 > \langle y\rangle > 0.25$. In fact, when sea quarks and antiquarks dominate over valence quarks, one might expect the averaged value of $(0.50 + 0.25)/2 = 0.375$ for $\langle y\rangle$, for both quarks and antiquarks.

TABLE III. For $A_{\rm eff}\Phi_{\nu_\mu} \propto E_\nu^{-\beta}$, average y, peak values for $(E^{\rm dep}/E_\nu)_{\rm peak}$ and $(E_\nu/E^{\rm dep})_{\rm peak}$. The WHM (Γ/E_ν) for fixed $E^{\rm dep}$ is $2^{1/(1+\beta)} - 1$, as explained in this Appendix.

E_ν	$\langle y\rangle$	$(E^{\rm dep}/E_\nu)_{\rm peak}$	$(E_\nu/E^{\rm dep})_{\rm peak}$
10 TeV	0.40	0.57	1.76
100 TeV	0.32	0.51	1.96
200 TeV	0.30	0.50	2.02
PeV	0.27	0.47	2.11
10 PeV	0.25	0.46	2.17
EeV	0.22	0.44	2.28
ZeV	0.20	0.42	2.36

However, for the sea quarks $\langle y\rangle$ is determined in part by nontrivial integration limits $y_{\rm min} > 0$, and $y_{\rm max} < 1$, and in part by the splitting functions of the partons. As a consequence, $\langle y\rangle$ may and does dip below 0.25 at energies $\gtrsim$ PeV. In [25] it is shown that $\langle y\rangle$ is 0.4, 0.32, 0.30, 0.27, and 0.22 at $E_\nu = 30$ TeV, 100 TeV, 200 TeV, 2 PeV, EeV

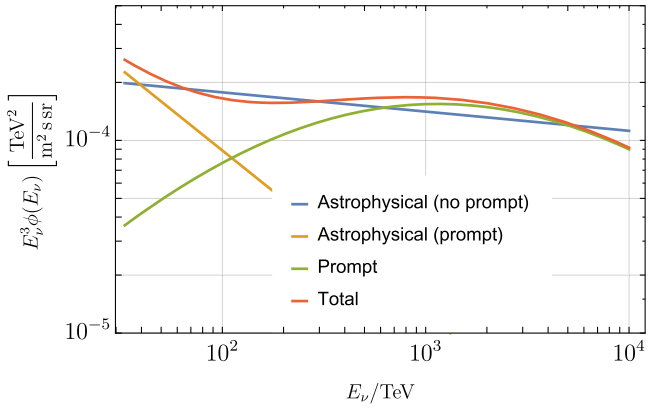

FIG. 20. Prompt (no veto), astrophysical and prompt + astrophysical total fluxes for the single-exponential (showers only).

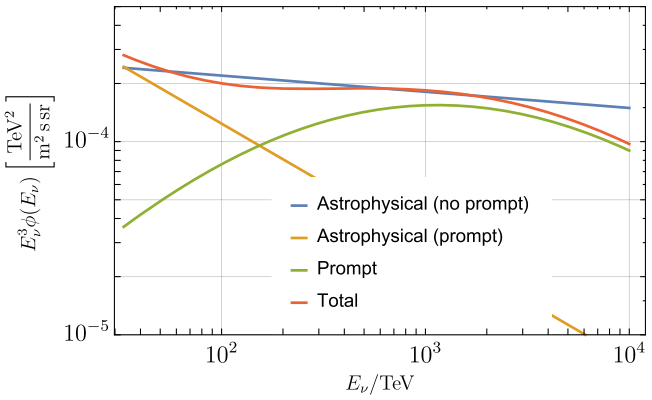

FIG. 21. Prompt (no veto), astrophysical and prompt + astrophysical total fluxes for the single-exponential (showers and tracks).

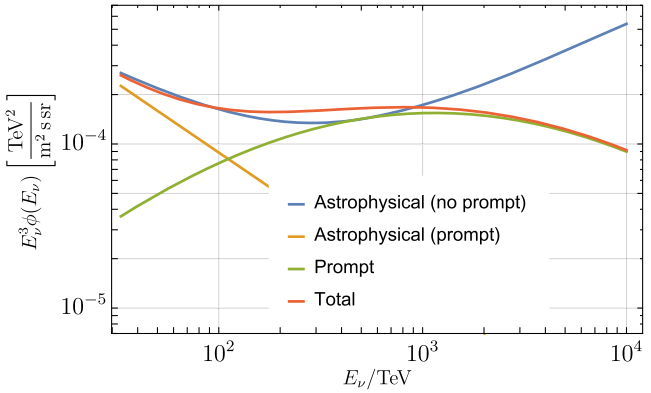

FIG. 22. Prompt (no veto), astrophysical and prompt + astrophysical total fluxes for the double-exponential (showers only).

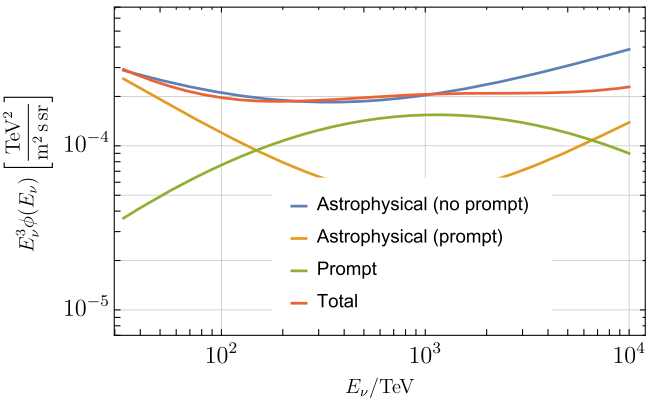

FIG. 23. Prompt (no veto), astrophysical and prompt + astrophysical total fluxes for the double-exponential (showers and tracks).

(10^3 PeV), respectively, and asymptotes at 0.20 above an EeV. The charged-current cross sections σ^ν_{CC} and $\sigma^{\bar\nu}_{CC}$ retain some memory of the valence quarks at 30 TeV, but are nearly equal above 100 TeV. In the weighting for $\langle y\rangle$, we have taken this into account. Values are given in Table III. These values, which validate the issue of energy transfer due to neutrino scattering raised in the previous section, correspond to a fractional energy $E_\mu(0)/E_\nu$ of $1 - \langle y\rangle = 0.6$, 0.65, 0.70, 0.75, and 0.8, respectively.[4] For the 30–100 TeV data set, we set the fractional energy $E_\mu(0)/E_\nu$ to 0.62, for the 100–200 TeV data set, to 0.67, and for the 200 TeV-2 PeV data set, to 0.72.

APPENDIX B: MUON SELF-VETO

The upper limit of the prompt flux cannot be directly used to predict the number of events as in (5). The veto

[4]At and above $E_\nu =$ a PeV, the fractional energy of the muon $E_\mu(0)$ rises slowly as $1 - \langle y\rangle = 0.75 + 0.01\log(E_\nu/\text{PeV})$, but these energies are beyond the concerns of the present work.

analysis technique implemented to avoid contamination of the sample by atmospheric neutrinos significantly reduces the *effective* flux that will produce prompt related events at IceCube. The prompt flux [43] has to be properly reduced, as described in [10,11], in order to use it with the usual effective areas. Although the north hemisphere flux remains unaltered by the veto, the southern flux is notably reduced, as can be seen in Fig. 8 of [10]. In this Appendix we stress the relevance of taking into account the veto technique.

In Figs. 20–23 we show the results of fitting the astrophysical flux with the total contribution of the prompt flux in the southern hemisphere, instead of the veto reduced one. There is not room to accommodate, in any case, an astrophysical flux through all the energy spectrum. The prompt flux reduction at low energies, where the statistics are higher, imposes that the astrophysical flux has to account for all the events in that zone. But the increase of the prompt flux at higher energies makes it impossible for the astrophysical flux to have soft exponents. Only in Fig. 23 does the astrophysical flux dominates again at the highest energies. But it is also unlikely that the prompt flux could account for the highest energy events, according to its small value.

[1] M. G. Aartsen *et al.* (IceCube Collaboration), First Observation of PeV-Energy Neutrinos with IceCube, Phys. Rev. Lett. **111**, 021103 (2013).

[2] S. Schonert, T. K. Gaisser, E. Resconi, and O. Schulz, Vetoing atmospheric neutrinos in a high energy neutrino telescope, Phys. Rev. D **79**, 043009 (2009); T. K. Gaisser, K. Jero, A. Karle, and J. van Santen, Generalized self-veto probability for atmospheric neutrinos, Phys. Rev. D **90**, 023009 (2014).

[3] M. G. Aartsen *et al.* (IceCube Collaboration), Evidence for high-energy extraterrestrial neutrinos at the IceCube detector, Science **342**, 1242856 (2013).

[4] L. A. Anchordoqui, H. Goldberg, M. H. Lynch, A. V. Olinto, T. C. Paul, and T. J. Weiler, Pinning down the cosmic ray source mechanism with new IceCube data, Phys. Rev. D **89**, 083003 (2014).

[5] M. G. Aartsen *et al.* (IceCube Collaboration), Atmospheric and astrophysical neutrinos above 1 TeV interacting in IceCube, Phys. Rev. D **91**, 022001 (2015).

[6] M. G. Aartsen *et al.* (IceCube Collaboration), Observation of High-Energy Astrophysical Neutrinos in Three Years of IceCube Data, Phys. Rev. Lett. **113**, 101101 (2014); M. G. Aartsen *et al.* (IceCube Collaboration), The IceCube neutrino observatory—Contributions to ICRC 2015 Part II: atmospheric and astrophysical diffuse neutrino searches of all flavors, arXiv:1510.05223.

[7] M. G. Aartsen *et al.* (IceCube Collaboration), Flavor Ratio of Astrophysical Neutrinos above 35 TeV in IceCube, Phys. Rev. Lett. **114**, 171102 (2015).

[8] S. Palomares-Ruiz, A. C. Vincent, and O. Mena, Spectral analysis of the high-energy IceCube neutrinos, Phys. Rev. D **91**, 103008 (2015).

[9] J. Van Santen (for the IceCube Collaboration), *Observations of the diffuse astrophysical neutrino flux with IceCube, in TeV Particle Astrophysics 2015*, (Kashiwa, Japan 2015).

[10] F. Halzen and L. Wille, Upper limit on forward charm contribution to atmospheric neutrino flux, arXiv:1601.03044.

[11] F. Halzen and L. Wille, On the charm contribution to the atmospheric neutrino flux, Phys. Rev. D **94**, 014014 (2016).

[12] M. G. Aartsen *et al.* (IceCube Collaboration), A combined maximum-likelihood analysis of the high-energy astrophysical neutrino flux measured with IceCube, Astrophys. J. **809**, 98 (2015).

[13] S. Razzaque, The Galactic center origin of a subset of IceCube neutrino events, Phys. Rev. D **88**, 081302 (2013); Y. Bai, A. J. Barger, V. Barger, R. Lu, A. D. Peterson, and J. Salvado, Neutrino lighthouse at Sagittarius A*, Phys. Rev. D **90**, 063012 (2014); L. A. Anchordoqui, Neutrino lighthouse powered by Sagittarius A* disk dynamo, Phys. Rev. D **94**, 023010 (2016).

[14] A. Neronov and D. V. Semikoz, Evidence the Galactic contribution to the IceCube astrophysical neutrino flux, Astropart. Phys. **75**, 60 (2016); A. Neronov and D. Semikoz, Galactic and extragalactic contributions to the astrophysical muon neutrino signal, Phys. Rev. D **93**, 123002 (2016); A. Palladino, M. Spurio, and F. Vissani, On the IceCube spectral anomaly, J. Cosmol. Astropart. Phys. 12 (2016) 045.

[15] M. G. Aartsen *et al.* (IceCube Collaboration), Observation and characterization of a cosmic muon neutrino flux from the Northern hemisphere using six years of IceCube data, Astrophys. J. **833**, 3 (2016).

[16] L. A. Anchordoqui *et al.*, Cosmic neutrino pevatrons: A brand new pathway to astronomy, astrophysics, and particle physics, JHEAp **1–2**, 1 (2014).

[17] H. N. He, R. Z. Yang, Y. Z. Fan, and D. M. Wei, TeV-PeV neutrinos over the atmospheric background: Originating from two groups of sources?, arXiv:1307.1450.

[18] C. Y. Chen, P. S. Bhupal Dev, and A. Soni, Two-component flux explanation for the high energy neutrino events at IceCube, Phys. Rev. D **92**, 073001 (2015).

[19] L. A. Anchordoqui, V. Barger, H. Goldberg, X. Huang, D. Marfatia, L. H. M. da Silva, and T. J. Weiler, IceCube neutrinos, decaying dark matter, and the Hubble constant, Phys. Rev. D **92**, 061301 (2015); Erratum, Phys. Rev. D **94**, 069901(E) (2016).

[20] M. Chianese, G. Miele, and S. Morisi, Dark matter interpretation of low energy IceCube MESE excess, J. Cosmol. Astropart. Phys. 01 (2017) 007.

[21] A. C. Vincent, S. Palomares-Ruiz, and O. Mena, Analysis of the 4-year IceCube high-energy starting events, Phys. Rev. D **94**, 023009 (2016).
[22] S. L. Glashow, Resonant scattering of antineutrinos, Phys. Rev. **118**, 316 (1960); V. S. Berezinsky and A. Z. Gazizov, Cosmic neutrinos and possibility to search for W bosons having 30-GeV-100-GeV masses in underwater experiments, Pis'ma Zh. Eksp. Teor. Fiz. **25**, 276 (1977) [JETP Lett. **25**, 254 (1977)].
[23] J. G. Learned and S. Pakvasa, Detecting tau-neutrino oscillations at PeV energies, Astropart. Phys. **3**, 267 (1995).
[24] S. W. Li, M. Bustamante, and J. F. Beacom, Echo technique to distinguish flavors of astrophysical neutrinos, arXiv: 1606.06290.
[25] R. Gandhi, C. Quigg, M. H. Reno, and I. Sarcevic, Ultrahigh-energy neutrino interactions, Astropart. Phys. **5**, 81 (1996).
[26] A. Cooper-Sarkar and S. Sarkar, Predictions for high energy neutrino cross-sections from the ZEUS global PDF fits, J. High Energy Phys. 01 (2008) 075; A. Cooper-Sarkar, P. Mertsch, and S. Sarkar, The high energy neutrino cross-section in the Standard Model and its uncertainty, J. High Energy Phys. 08 (2011) 042.
[27] M. G. Aartsen *et al.* (IceCube Collaboration), Measurement of the Atmospheric ν_e Flux in IceCube, Phys. Rev. Lett. **110**, 151105 (2013).
[28] R. Abbasi *et al.* (IceCube Collaboration), First search for atmospheric and extraterrestrial neutrino-induced cascades with the IceCube detector, Phys. Rev. D **84**, 072001 (2011).
[29] F. Halzen (private communication).
[30] V. Barger, L. Fu, J. G. Learned, D. Marfatia, S. Pakvasa, and T. J. Weiler, Glashow resonance as a window into cosmic neutrino sources, Phys. Rev. D **90**, 121301 (2014); D. Biehl, A. Fedynitch, A. Palladino, T. J. Weiler, and W. Winter, Astrophysical neutrino production diagnostics with the Glashow resonance, J. Cosmol. Astropart. Phys. 01 (2017) 033.
[31] E. Waxman and J. N. Bahcall, High-energy neutrinos from astrophysical sources: An upper bound, Phys. Rev. D **59**, 023002 (1998).
[32] M. Ackermann *et al.* (Fermi-LAT Collaboration), The spectrum of isotropic diffuse gamma-ray emission between 100 MeV and 820 GeV, Astrophys. J. **799**, 86 (2015).
[33] K. Murase, M. Ahlers, and B. C. Lacki, Testing the hadronuclear origin of PeV neutrinos observed with IceCube, Phys. Rev. D **88**, 121301 (2013).
[34] L. A. Anchordoqui, H. Goldberg, F. Halzen, and T. J. Weiler, Galactic point sources of TeV antineutrinos, Phys. Lett. B **593**, 42 (2004); L. A. Anchordoqui, Neutron β-decay as the origin of IceCubes PeV (anti)neutrinos, Phys. Rev. D **91**, 027301 (2015).
[35] K. Mannheim, R. J. Protheroe, and J. P. Rachen, On the cosmic ray bound for models of extragalactic neutrino production, Phys. Rev. D **63**, 023003 (2000).
[36] L. A. Anchordoqui, H. Goldberg, F. Halzen, and T. J. Weiler, Neutrinos as a diagnostic of high energy astrophysical processes, Phys. Lett. B **621**, 18 (2005).
[37] M. G. Aartsen *et al.* (IceCube Collaboration), IceCube-Gen2: A vision for the future of neutrino astronomy in Antarctica, arXiv:1412.5106.
[38] A. Neronov, D. V. Semikoz, L. A. Anchordoqui, J. Adams, A. V. Olinto, and E. Parizot, Sensitivity of the space-based CHerenkov from Astrophysical Neutrinos Telescope (CHANT), Phys. Rev. D **95**, 023004 (2017).
[39] E. Fermi, On the origin of the cosmic radiation, Phys. Rev. **75**, 1169 (1949).
[40] V. Barger, Y. Gao, and D. Marfatia, Dark matter at DeepCore and IceCube, Phys. Rev. D **83**, 055012 (2011).
[41] T. K. Gaisser, F. Halzen, and T. Stanev, Particle astrophysics with high-energy neutrinos, Phys. Rep. **258**, 173 (1995); Erratum, Phys. Rep. **271**, 355(E) (1996).
[42] M. C. Gonzalez-Garcia and F. Halzen, Gamma ray burst neutrinos probing quantum gravity, J. Cosmol. Astropart. Phys. 02 (2007) 008.
[43] F. Halzen and L. Wille (private communication).